Control of spin-orbit torques through magnetic symmetry in differently oriented noncollinear antiferromagnetic Mn_3Pt

H. Bai,[1,*] X. F. Zhou,[1,*] H. W. Zhang,[2] W. W. Kong,[2] L. Y. Liao,[1] X. Y. Feng,[2] X. Z. Chen,[1] Y. F. You,[1] Y. J. Zhou,[1] L. Han,[1] W. X. Zhu,[1] F. Pan,[1] X. L. Fan,[2,†] and C. Song[1,‡]

[1]*Key Laboratory of Advanced Materials, School of Materials Science and Engineering, Tsinghua University, Beijing 100084, China*

[2]*The Key Lab for Magnetism and Magnetic Materials of Ministry of Education, Lanzhou University, Lanzhou 730000, China*

(Received 29 April 2021; revised 2 August 2021; accepted 13 August 2021; published 1 September 2021)

Interconversion of charge and spin currents via spin Hall effect is one of the key physical phenomena in spintronics. However, the spin polarizations are orthogonal to both the charge and spin flows due to the restricted symmetry conditions. Here, we use noncollinear antiferromagnet Mn_3Pt, which has different magnetic mirror planes in different orientations, to investigate magnetic symmetry dependent atypical spin-orbit torques. We observed weak generation of out of plane spin polarization (σ_z) in Mn_3Pt/permalloy bilayers when current was applied perpendicular to the magnetic mirror plane of Mn_3Pt, and strong generation of σ_z when current was applied parallel to the magnetic mirror plane. All three oriented Mn_3Pt films show the same pattern, indicating the generation of unconventional σ_z has strong dependence on magnetic symmetry. Controlling spin-orbit torques by changing current directions in differently oriented Mn_3Pt films provides a strategy for optimizing antiferromagnetic spintronics.

DOI: 10.1103/PhysRevB.104.104401

I. INTRODUCTION

For seeking nonvolatile memories with high speed, high density, and low power consumption, the next-generation magnetic memories have been intensively investigated. Wherein, current-induced spin-orbit torque (SOT) is one of the most important topics because the torque can be used to switch magnetization [1–5]. Various materials, such as heavy metals (HMs) [1,3], topological insulators [6], two-dimensional materials [7], and antiferromagnets (AFMs) [8], have been used as the source of SOT. In the classic picture of SOT induced by spin Hall effect (SHE), charge currents flowing along the in-plane direction (x direction) can generate out of plane spin currents (flowing in the z direction) with spin polarization σ along the y direction (σ_y). Such an orthogonal relation is not satisfied in materials with low-symmetric crystalline structure, where both the spin flow and spin polarization can be along the z direction (σ_z) when a current goes through the x axis [9–12]. For materials with high-symmetric crystalline structure, other low-symmetric elements such as the ordered magnetic moments can also give rise to the generation of σ_z [13–15]. Those efforts would further improve the dimension of SOTs in electrical control of magnetic moments, as well as the efficiency of spintronics devices.

Recently, crystal symmetry dependent field-free SOT switching of perpendicular magnetization was reported in a CuPt/CoPt bilayer, where CuPt is a heavy metal alloy with a low-symmetry point group. In this system, SOT switching strongly depends on the relative orientation between the current flow and the crystal symmetry of CuPt [16]. For high crystal symmetric materials, it is pursued to investigate magnetic symmetry dependent atypical spin current, which can be achieved by applying current along different magnetic orientations.

Noncollinear AFMs have triangular spin structure with magnetic moments aligned in the kagome plane. The special magnetic structure gives rise to abundant transport phenomenon [17,18] and effective charge-spin conversion [8]. Mn_3Pt is a typical noncollinear AFM with Néel temperature $T_N \sim 475$ K. The crystal structure of Mn_3Pt is face-centered cubic (fcc), where Mn atoms are at face-centered positions. Magnetic moments of Mn atoms in a (111) kagome plane are aligned 120 ° to each other [19,20], which can reduce the magnetic symmetry [13]. Thus, Mn_3Pt has the potential to generate spin current with different spin polarization directions as well as atypical spin torques, which would strongly depend on the relative direction of the current flow and the magnetic symmetry of Mn_3Pt.

In this work, we study the influence of facet and crystallographic direction on the current-induced atypical spin torques in noncollinear AFM Mn_3Pt by spin torque ferromagnetic resonance (ST FMR). Different from the in-plane spin polarization (σ_y) induced by conventional SHE, out of plane spin polarization may exist in Mn_3Pt, which is related to the magnetic symmetry. As shown in Fig. 1, when the current is parallel to the magnetic mirror plane of Mn_3Pt, out of plane spin polarization (σ_z) is allowed; otherwise, when the current is perpendicular to the magnetic mirror plane, σ_z is forbidden. We demonstrate that the atypical spin polarization has dependence on the facet and crystallographic direction of Mn_3Pt, enabling the manipulation of spin polarization by just changing the current directions, which would advance the understanding of the anisotropic spin current generation in

*These authors contributed equally to this work.
†fanxiaolong@lzu.edu.cn
‡songcheng@mail.tsinghua.edu.cn

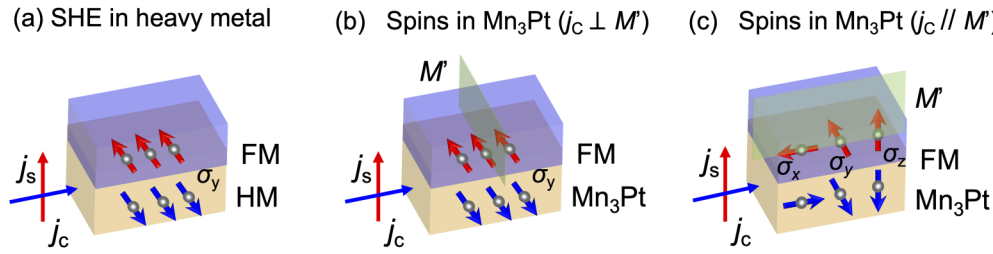

FIG. 1. Schematics of (a) conventional spin Hall effect in heavy metal, (b) spin generation in Mn_3Pt with current perpendicular to the magnetic mirror plane ($j_C \perp M'$), and (c) spin generation in Mn_3Pt with current parallel to the magnetic mirror plane ($j_C \parallel M'$). Here, blue arrows (j_C) represent charge current; red arrows (j_S) represent spin current. M' represents the magnetic mirror plane.

noncollinear AFM as well as pave the way for controllable SOT.

II. EXPERIMENTS

Mn_3Pt films of 20 nm thickness were deposited on MgO substrates at 573 K by dc magnetron sputtering with a vacuum of 2×10^{-5} Pa. After the deposition, Mn_3Pt films were *in situ* annealed at 873 K for 1 h. The x-ray diffraction (XRD) results show that Mn_3Pt films are well crystallized and have (100), (110), and (111) orientations when grown on MgO (100), (110), and (111) substrates, respectively (see Supplemental Material, Fig. S1 [21]. All the films are single phase and quasiepitaxial growth. Magnetic hysteresis loops of Mn_3Pt films were measured by a superconducting quantum interference device (SQUID). Saturation magnetizations (M_S) of all oriented Mn_3Pt films are about 10 emu/cm^3, revealing that our Mn_3Pt films are antiferromagnetic, as shown in Fig. S3 [21]. The good growth of multioriented Mn_3Pt films provides a precondition for the study of facet-dependent SOT in Mn_3Pt as discussed below.

Mn_3Pt (12 nm)/permalloy ($Ni_{80}Fe_{20}$, 10 nm) bilayers were grown and patterned into microstrip devices with a length of 50 μm and a width of 20 μm by standard photolithography and Ar-ion milling techniques. Top electrodes of Ti (10 nm)/Au (50 nm) were deposited by *e*-beam evaporation. After the lift-off, the fabrication is completed, and the optical image is shown in Fig. 2(a). In order to investigate the dependence on magnetic symmetry, we fabricated different directional ST FMR devices [Fig. 2(a)]. The current direction can be controlled parallel or perpendicular to the magnetic mirror by controlling the direction of ST-FMR microstrips. The calibration of relative orientation between applied current and the magnetic mirror plane is discussed in the Supplemental Material [21]. ST FMR measurements were carried out by injecting a microwave current into the Mn_3Pt/permalloy (Py) bilayers. Figure 2(b) shows the schematic diagram of ST FMR measurement. A magnetic field H was applied in the sample plane and at an angle φ to the current direction. Spin torques generated by the charge current excited the precession of the magnetic moment of Py. The anisotropy magnetoresistance (AMR) of the precessing magnetic moment induces electrical resistance oscillating at the same frequency as the rf current, which ultimately gives rise to dc voltage due to the rectification effect. The rectified voltage was detected by a lock-in amplifier.

III. RESULTS

A. Magnetic configuration analysis of Mn_3Pt

Noncollinear antiferromagnet Mn_3Pt has two possible magnetic structures, T_1 and T_2 [19,20], as shown in Fig. 2(c). For the T_1 configuration, magnetic moments of Mn atoms are aligned head to head or tail to tail, while for the T_2 configuration, magnetic moments of Mn atoms are aligned head to tail. Note that the energy difference between T_1 and T_2 configurations is very tiny and sensitive to epitaxial strain [22]. Strain in our Mn_3Pt film is about 0.8%, larger than the strain induced by ferroelectric substrates [23]. Detailed calculation is discussed in the Supplemental Material [21]. The anomalous Hall effect (AHE) provides a criterion for distinguishing the two magnetic configurations. Theoretical and experimental results show that noncollinear AFM with the T_1 configuration presents robust AHE, whereas AFM with the T_2 configuration presents no AHE, in both the Mn_3X (X = Rh, Ir, Pt) [24–26] and the antiperovskite Mn_3YN (Y = Ga, Zn, Ag, Ni, etc.) [27–29]. As shown in Fig. 2(d), the dependence of Hall resistance on magnetic field in our (100)- oriented Mn_3Pt film presents only a straight line, revealing the contribution of AHE is absent. Therefore we consider our grown Mn_3Pt has the T_2 configuration.

B. Symmetry analysis of atypical out of plane spin polarization

ST FMR spectra of Mn_3Pt (12 nm)/Py (10 nm) are obtained using the standard ST FMR setup. Figure 3(b) shows a typical ST FMR spectrum; the resonance peaks can be well fitted by the following equation [30]:

$$V(H) = V_S \frac{\Delta H^2}{\Delta H^2 + (H - H_0)^2} + V_A \frac{\Delta H (H - H_0)}{\Delta H^2 + (H - H_0)^2}, \tag{1}$$

where ΔH (H_0) is the width (position) of the resonance peak. The first term represents a symmetric Lorentzian line shape with an amplitude V_S; the second term corresponds to an antisymmetric line shape with an amplitude V_A.

We perform an angle-dependent measurement to investigate the property of the torque acting on Py when a charge current is passed through the Mn_3Pt. According to the spin rectification theory for AMR, the intensity of V_S (V_A) depends on the product of the angular related AMR ($\sim \sin 2\varphi$) and in-plane (out of plane) torque [31]. For example, for the simple Pt/Py bilayer, the current-induced dampinglike torque $m \times \sigma_y \times m$ produces an in-plane torque with dependence of $\cos\varphi$,

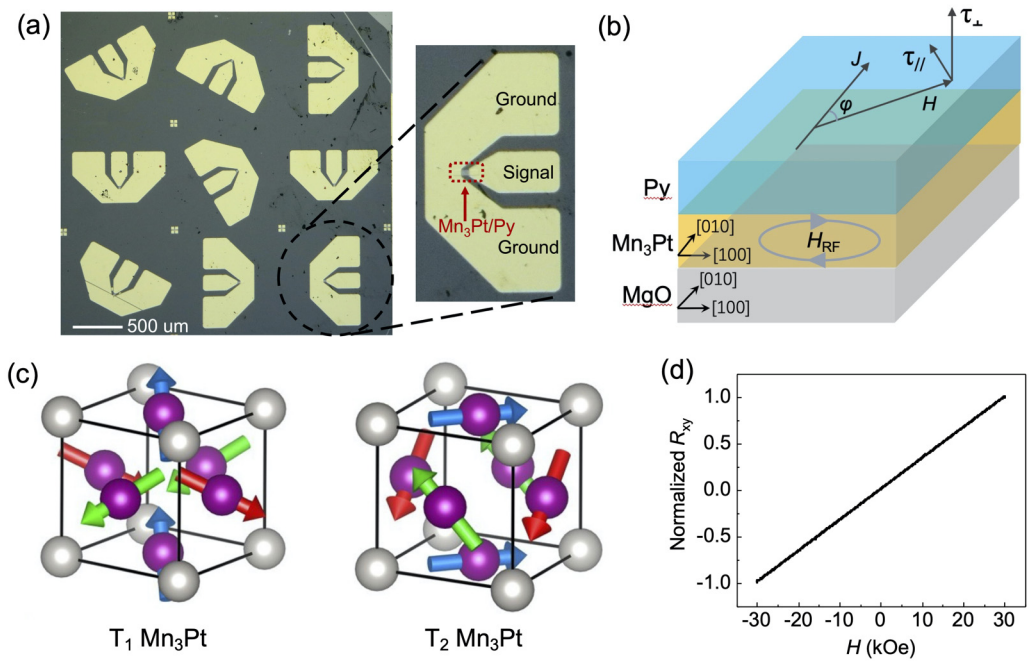

FIG. 2. (a) Optical images of ST FMR devices along different orientations on the same film. (b) The schematic diagram for ST FMR device of Mn_3Pt/Py bilayer with spin torques. (c) The schematic magnetic structures of T_1 and T_2 Mn_3Pt. (d) The normalized Hall resistance recorded as a function of magnetic field in our grown (100)-oriented Mn_3Pt film.

hence the amplitude of $V_S = S \sin 2\varphi \cos\varphi$ [31]. The current-induced Oersted field produces an out of plane torque $m \times \sigma_y$, leading to $V_A = A \sin 2\varphi \cos\varphi$ [31]. V_S and V_A show same angular dependence for the simple heavy metal/ferromagnet system, where the in-plane spin polarization (σ_y) is mainly caused by conventional SHE.

The low magnetic symmetry of Mn_3Pt can induce the generation of σ_z and result in additional torque terms. In this case, angular dependences of both V_S and V_A are different from the conventional $\sim\sin2\varphi\cos\varphi$. The fieldlike torque of σ_z contributes to V_S by an additional term ($B\sin2\varphi$), while the dampinglike torque of σ_z contributes to V_A by an additional term ($C\sin2\varphi$). B and C are constant terms. Thus, the ST FMR signal of the Mn_3Pt/Py bilayer can be well fitted by simply adding a term to V_S and V_A:

$$V_S = S \sin 2\varphi \cos\varphi + B \sin 2\varphi, \tag{2}$$

$$V_A = A \sin 2\varphi \cos\varphi + C \sin 2\varphi, \tag{3}$$

where S, A, B, and C are amplitudes of different angular-dependent contributions of the ST FMR signal. The angular dependences for the in-plane ($\tau_\parallel$) and out of plane torque ($\tau_\perp$) have the following forms:

$$\tau_\parallel(\varphi) = \tau_S \cos\varphi + \tau_B, \tag{4}$$

$$\tau_\perp(\varphi) = \tau_A \cos\varphi + \tau_C, \tag{5}$$

where τ_S, τ_A, τ_B, and τ_C are independent of φ. The $\tau_S \cos\varphi$ represents the contribution of the dampinglike torque of $\sigma_y \propto m \times \sigma_y \times m$, $\tau_A \cos\varphi$ represents the contribution from Oersted field torque $\propto m \times h$ and fieldlike torque of $\sigma_y \propto m \times \sigma_y$, both two terms are widely observed in heavy metal/ferromagnet system. The new terms, τ_B and τ_C, correspond to in-plane fieldlike torque of $\sigma_z \propto m \times \sigma_z$ and out of plane dampinglike torque of $\sigma_z \propto m \times \sigma_z \times m$, respectively. We discuss in detail the angular dependences of the Oersted field and all possible spin torques in the Supplemental Material [21].

Then broken symmetry is the prerequisite for the generation of σ_z, where a crystal mirror (M) or a magnetic mirror (M') is the key element for the analysis of broken symmetry. The M' is different from M, because M' contains time-reversal symmetry T; i.e., $M' = MT$ [5,9,13]. In this case, both axial vectors and polar vectors show the same pattern: Becoming revised if perpendicular to M' and staying unchanged if parallel to M' [5,13], for example, $E_\perp \to -E_\perp$, $E_\parallel \to E_\parallel$. Spin torque τ is a pseudovector, so it stays unchanged after the magnetic mirror operation ($\tau_\perp \to \tau_\perp$, $\tau_\parallel \to \tau_\parallel$) [13]. Detailed analysis of the magnetic mirror operation is shown in the Supplemental Material [21]. Since SOT is a function of electric field E and relative angle φ, i.e., $\tau = \tau\,(E, \varphi)$, the effects of M'on the three parameters (τ, E, φ) cause constraints on τ.

According to the Fourier formula, the spin-orbit torques $\tau_\parallel(E, \varphi)$ and $\tau_\perp(E, \varphi)$ can be expanded in the following forms [9,13]:

$$\tau_\parallel(E, \varphi) = E[S_0 + S_1\cos(\varphi) + S_2\sin(\varphi) + S_3\cos(2\varphi) + S_4\sin(2\varphi) + \cdots], \tag{6}$$

$$\tau_\perp(E, \varphi) = E[A_0 + A_1\cos(\varphi) + A_2\sin(\varphi) + A_3\cos(2\varphi) + A_4\sin(2\varphi) + \cdots]. \tag{7}$$

According to the angular dependence in Eqs. (4) and (5), the ES_0 and EA_0 terms, respectively, represent the fieldlike and dampinglike torque of σ_z.

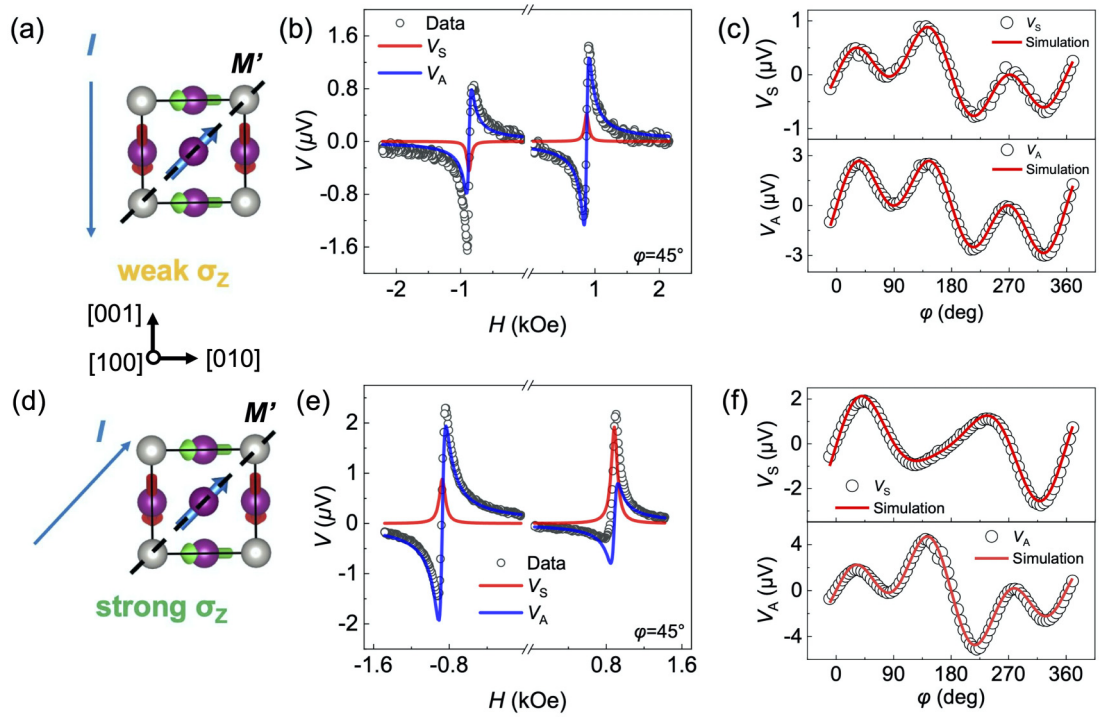

FIG. 3. Current direction dependent σ_z in (100)-oriented Mn_3Pt. (a) The schematic of magnetic configuration and current direction. The long blue arrow represents the direction of applied current. Short red, blue, and green arrows represent magnetic moments of Mn atoms, which are perpendicular to each other. The black dashed line represents the magnetic mirror plane. In this case, the current along the [001] direction is 45° from the magnetic mirror plane. (b) ST FMR resonances under positive and negative magnetic field with $\varphi = 45°$. Here, circles are measured data; red and blue lines are, respectively, symmetric and antisymmetric components of the raw data, which are fitted by Eq. (1). (c) In-plane magnetic field angular dependence of symmetric (V_S) and antisymmetric line shape (V_A). Red lines represent the simulation lines fitted by Eq. (2) or (3). Results of (b), (c) are measured for current tilted to the magnetic mirror plane at 45 °. (d) The schematic for the current along the [011] direction, which is parallel to the magnetic mirror plane. (e) ST FMR resonances under positive and negative magnetic field with $\varphi = 45°$. (f) In-plane magnetic field angular dependence of symmetric (V_S) and antisymmetric line shape (V_A). Results of (e), (f) are measured for current parallel to the magnetic mirror plane.

When $E \perp M'$, after the magnetic mirror operation, $E \rightarrow -E$, $\varphi \rightarrow -\varphi$ (analyzed in the Supplemental Material [21]),

$$\tau_{\parallel}(-E, -\varphi) = -E[S_0 + S_1\cos(-\varphi) + S_2\sin(-\varphi) + S_3\cos 2(-\varphi) + S_4\sin 2(-\varphi) + \cdots]. \quad (8)$$

Because $\tau_{\parallel}(E, \varphi) = \tau_{\parallel}(E, -\varphi)$, we get

$$S_0 + S_2\sin\varphi + S_4\sin 2\varphi = 0, \quad (9)$$

so that

$$\tau_{\parallel}(E, \varphi) = E[S_1\cos\varphi + S_3\cos(2\varphi) + \cdots]. \quad (10)$$

Similarly, the out of plane torque presents analogous forms:

$$\tau_{\perp}(E, \varphi) = E[A_1\cos\varphi + A_3\cos(2\varphi) + \cdots], \quad (11)$$

where S_0 and A_0 are zero and the generation of σ_z is not allowed.

When $E \parallel M'$, after the magnetic mirror operation, $E \rightarrow E$, $\varphi \rightarrow -\varphi$ (analyzed in the Supplemental Material [21]),

$$\tau_{\parallel}(E, -\varphi) = E[S_0 + S_1\cos(-\varphi) + S_2\sin(-\varphi) + S_3\cos 2(-\varphi) + S_4\sin 2(-\varphi) + \cdots]. \quad (12)$$

Because $\tau_{\parallel}(E, \varphi) = \tau_{\parallel}(E, -\varphi)$, we get

$$S_2\sin\varphi + S_4\sin 2\varphi = 0, \quad (13)$$

so that

$$\tau_{\parallel}(E, \varphi) = E[S_0 + S_1\cos\varphi + S_3\cos(2\varphi) + \cdots]. \quad (14)$$

Similarly,

$$\tau_{\perp}(E, \varphi) = E[A_0 + A_1\cos\varphi + A_3\cos(2\varphi) + \cdots], \quad (15)$$

where S_0 and A_0 are not zero and the generation of σ_z is allowed.

In summary, when $E \perp M'$, σ_z-induced fieldlike torque (τ_B) and dampinglike torque (τ_C) are theoretically absent. But when $E \parallel M'$, σ_z-induced τ_B and τ_C are theoretically existent.

C. Experimental results of magnetic symmetry dependent SOT

For (100)-oriented Mn_3Pt, the magnetic configuration is shown in Figs. 3(a) and 3(d), from which we can find the mirror plane is the $(01\bar{1})$ plane. In order to investigate the dependence of SOT on the magnetic symmetry, ST FMR measurements were carried out in two different directional devices, with current applied along the [001] and [011] directions, as shown in Figs. 3(a) and 3(d). We first show the ST FMR spectra under positive and negative magnetic field

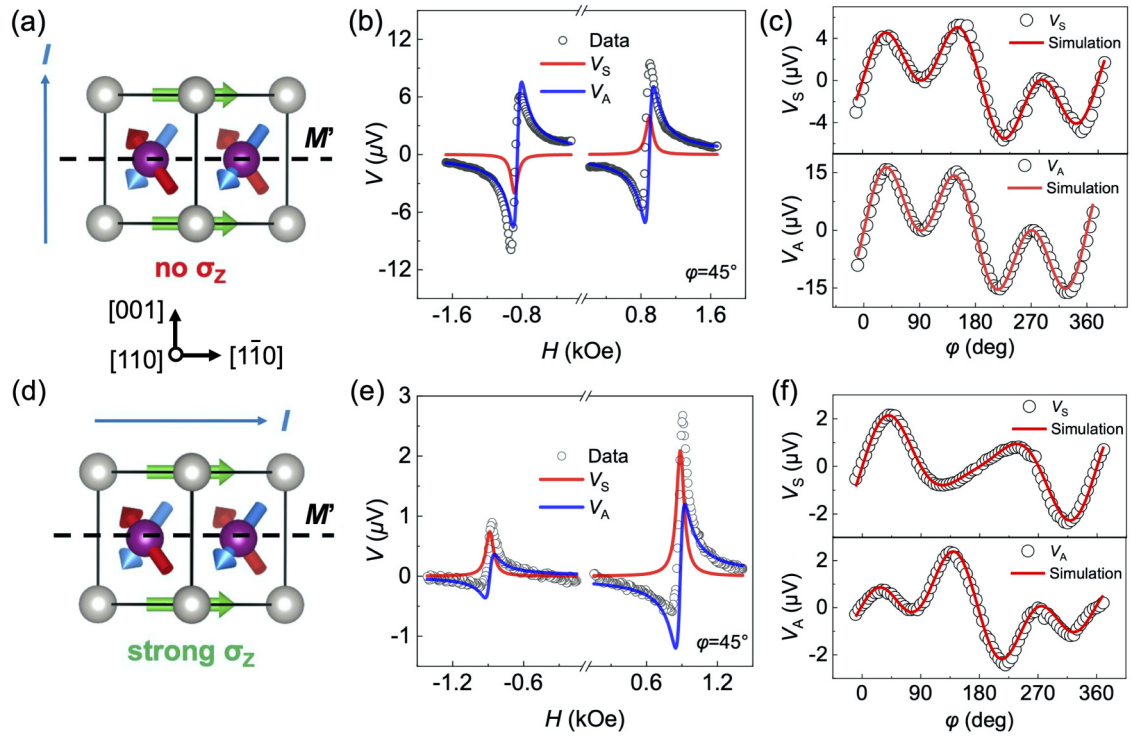

FIG. 4. Current direction dependent σ_z in (110)-oriented Mn_3Pt. (a) The schematic of magnetic configuration and current direction. The current direction along [001] is perpendicular to the magnetic mirror plane. (b) ST FMR resonances under positive and negative magnetic field with $\varphi = 45°$. (c) In-plane magnetic field angular dependence of symmetric (V_S) and antisymmetric line shape (V_A). Results of (b), (c) are measured for the current direction perpendicular to the magnetic mirror plane. (d) The schematic for the current along the [1$\bar{1}$0] direction, which is parallel to the magnetic mirror plane. (e) ST FMR resonances under positive and negative magnetic field with $\varphi = 45°$. (f) In-plane magnetic field angular dependence of symmetric (V_S) and antisymmetric line shape (V_A). Results of (e), (f) are measured for the current direction parallel to the magnetic mirror plane.

measured at $\varphi = 45°$ in Figs. 3(b) and 3(e). The symmetric line shape (V_S) and antisymmetric line shape (V_A) are fitted by Eq. (1); the corresponding results are depicted as red and blue lines in Figs. 3(b) and 3(e). According to the above analysis of angular dependence ($\sim \sin 2\varphi \cos\varphi$ for σ_y and $\sim \sin 2\varphi$ for σ_z), conventional σ_y-induced V_S and V_A have opposite signs with the same amplitudes at positive ($\varphi = 45°$) and negative magnetic field ($\varphi = 225°$), while the unconventional σ_z-induced V_S and V_A have the same sign and amplitudes at positive and negative magnetic field. Comparing the sign and amplitude of V_S and V_A under positive and negative magnetic field may qualitatively reveal whether σ_z exists.

For the case of current tilted 45° to the magnetic mirror plane, both V_S and V_A show opposite sign and nearly the same amplitude under positive and negative magnetic field [Fig. 3(b)], indicating the robust contribution of σ_y and weak contribution of σ_z. In the scenario of current parallel to the magnetic mirror, it is clear that V_S under positive and negative magnetic field has the same sign [Fig. 3(e)], implying strong fieldlike torque of σ_z (τ_B). Although V_A has the same sign under positive and negative magnetic field, the amplitudes are different [Fig. 3(e)], which is possibly caused by the superposition of σ_y-induced fieldlike torque and σ_z-induced dampinglike torque (τ_C). In order to calculate the relative intensity of σ_y and σ_z, angle-dependent ST FMR measurements were carried out for the same devices, i.e., current tilted 45° and parallel to the magnetic mirror plane. ST FMR spectra under distinct angles are fitted by Eq. (1) to get angle-dependent V_S and V_A, as shown in Figs. 3(c) and 3(f). The angle-dependent V_S and V_A can be well fitted by Eq. (2) or (3), as depicted with red lines in Figs. 3(c) and 3(f). A detailed discussion about the separation of V_S and V_A as well as the amplitudes of σ_y- and σ_z-induced spin torques is presented in the Supplemental Material [21]. After the simulation, contributions from different spin polarization can be distinguished, giving rise to the fieldlike (τ_B/τ_A) and dampinglike torque ratios (τ_C/τ_S) between σ_z and σ_y. In detail, the values of τ_B/τ_A are, respectively, 0.041 and 0.363 for current along the [001] and [011] directions of Mn_3Pt; τ_C/τ_S are, respectively, 0.222 and 1.358 for current along the [001] and [011] directions of Mn_3Pt. Obviously, the σ_z-induced spin torques are much stronger for current along the [011] direction (parallel to the magnetic mirror plane) than that along the [001] direction (45° tilted to the magnetic mirror plane) in (100)-oriented Mn_3Pt, which is consistent with the above symmetry analysis.

To prove the generation of σ_z is commonly dependent on the current direction in Mn_3Pt, we carried out ST FMR measurements and got the fitted V_S and V_A in both (110)- and (111)-oriented Mn_3Pt. For (110)-oriented Mn_3Pt, the magnetic structure is shown in Figs. 4(a) and 4(d); the magnetic mirror plane of (001) is depicted as a black dashed line. When current flows perpendicular to the magnetic mirror plane (i.e.,

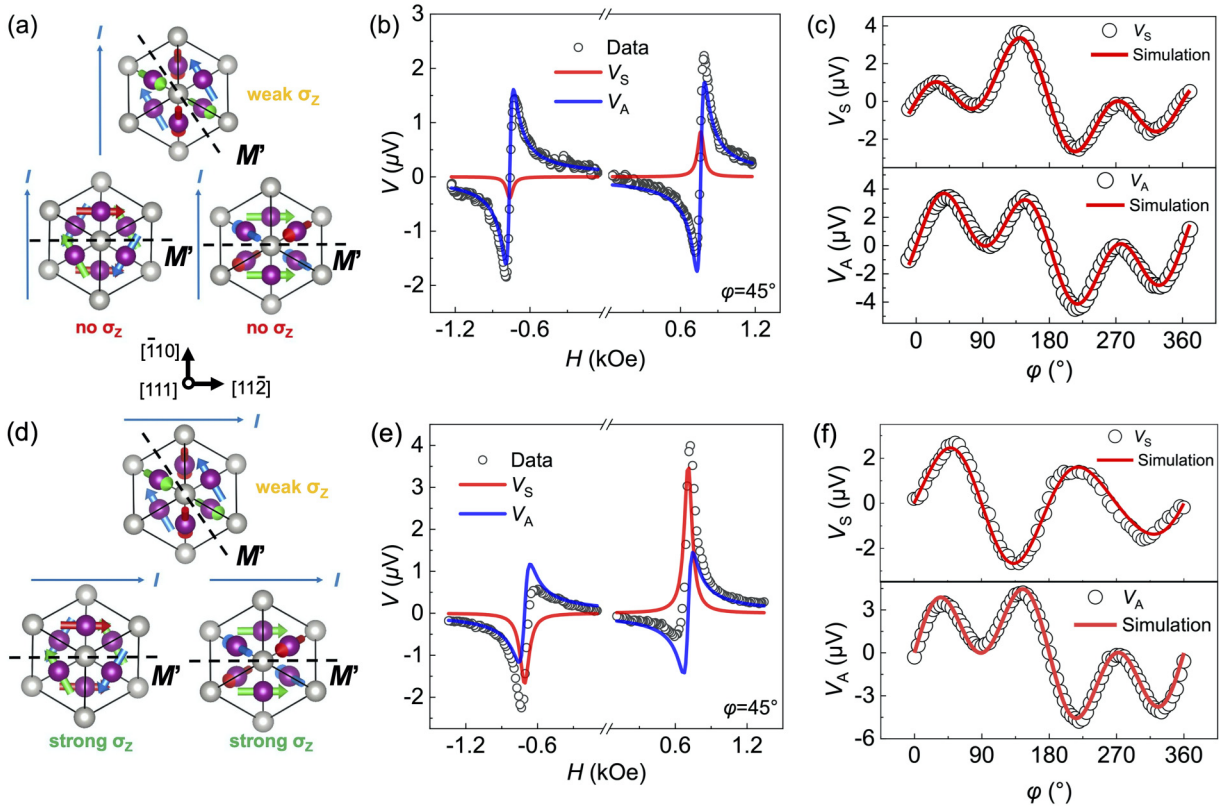

FIG. 5. Symmetry-dependent σ_z in (111)-oriented Mn_3Pt. (a) The schematic of magnetic configurations and current direction. Three magnetic configurations are degenerate for (111)-oriented Mn_3Pt. For two configurations at the bottom panel, current along the $[11\bar{2}]$ direction is perpendicular to the magnetic mirror; σ_z is absent. The orthogonal relation is not satisfied for another configuration, giving rise to weak σ_z. (b) ST FMR resonances under positive and negative magnetic field with $\varphi = 45^\circ$. (c) In-plane magnetic field angular dependence of symmetric (V_S) and antisymmetric line shape (V_A). Results of (b), (c) are measured for the current direction mainly perpendicular to the magnetic mirror plane. (d) The schematic for the current direction mainly parallel to the magnetic mirror plane. For two configurations at the bottom panel, current along the $[1\bar{1}0]$ direction is parallel to the magnetic mirror, giving rise to strong σ_z. The parallel relation is not available for another configuration, giving rise to weak σ_z. (e) ST FMR resonances under positive and negative magnetic field with $\varphi = 45^\circ$. (f) In-plane magnetic field angular dependence of symmetric (V_S) and antisymmetric line shape (V_A). Results of (e), (f) are measured for the current direction mainly parallel to the magnetic mirror plane.

[001] direction), V_S and V_A in Fig. 4(b) both show opposite signs and nearly the same amplitude under positive and negative magnetic field, revealing the σ_z is absent. Differently, when current flows parallel to the magnetic mirror (i.e., $[1\bar{1}0]$ direction), the signs of V_S under positive and negative magnetic field are the same, indicating that the contribution of σ_z-induced fieldlike torque is obvious. The different amplitude of V_A reveals the σ_y-induced fieldlike torque and σ_z-induced dampinglike torque coexist. Figures 4(c) and 4(f) illustrate angle-dependent V_S and V_A as well as the fitting results (red lines). The simulation used by Eqs. (2) or (3) gives rise to τ_B/τ_A of 0.026 and 0.722, respectively, for current along the [001] and $[1\bar{1}0]$ directions of Mn_3Pt. Similarly, the value of τ_C/τ_S is calculated as 0.079 and 0.735, respectively, for current along the [001] and $[1\bar{1}0]$ directions of Mn_3Pt. Obviously, the generation of σ_z is much larger when the current is along the $[1\bar{1}0]$ direction (parallel to the magnetic mirror plane) than when it is along the [001] direction (perpendicular to the mirror plane) in (110)-oriented Mn_3Pt, which is consistent with the pattern of (100)-oriented Mn_3Pt.

For (111)-oriented Mn_3Pt, three possible magnetic configurations coexist, as shown in Figs. 5(a) and 5(d), where the magnetic mirror planes belong to the {112} crystal plane family. For the configurations of the bottom panel in Fig. 5(a), current along the $[11\bar{2}]$ direction is perpendicular to the magnetic mirror planes, the generation of σ_z is theoretically forbidden. Only weak σ_z can be generated for the top configuration in Fig. 5(a). In contrast, strong σ_z can be generated for the bottom configurations of Fig. 5(d), giving rise to robust σ_z when the current is along the $[1\bar{1}0]$ axis. ST FMR spectra measured at $\varphi = 45^\circ$ are shown in Figs. 5(b) and 5(e). After comparing the sign and amplitude under positive and negative magnetic field, it is found the σ_z-induced spin torques are existent (absent) for current along the $[1\bar{1}0]$ ($[11\bar{2}]$) directions, which supports the above analysis. Figures 5(c) and 5(f) illustrate angle-dependent symmetric (V_S) and antisymmetric line shape (V_A), from which we can get the value of τ_B/τ_A and τ_C/τ_S. As displayed in Table S2 in the Supplemental Material [21], τ_B/τ_A for current along the $[11\bar{2}]$ and $[1\bar{1}0]$ directions are, respectively, 0.203 and 0.412; τ_C/τ_S for current along the $[11\bar{2}]$ and $[1\bar{1}0]$ directions are, respectively, 0.083 and 1.679. Both σ_z-induced fieldlike (τ_B) and dampinglike (τ_C) torques are larger when the current is parallel to the magnetic mirror plane than when it is perpendicular to the magnetic mirror

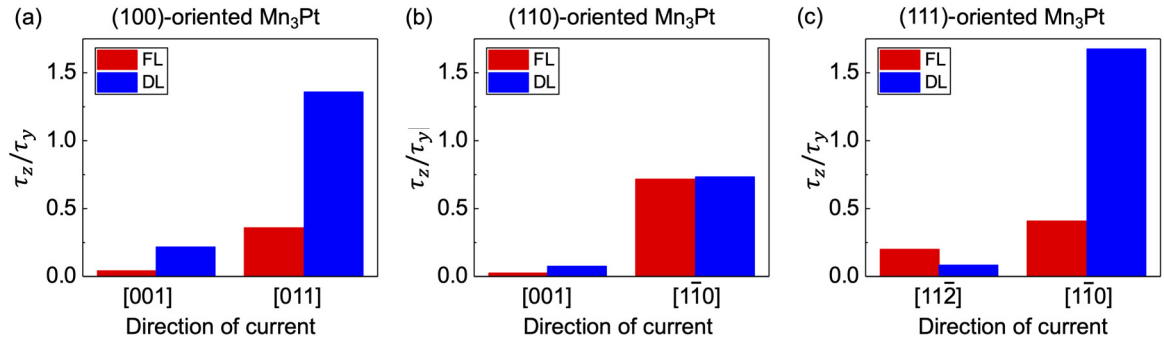

FIG. 6. Summaries of ratios between σ_z-induced and σ_y-induced spin torques (τ_z/τ_y) when the current is along different crystallographic directions in (a) (100)-, (b) (110)-, and (c) (111)-oriented Mn_3Pt. Red and blue columns, respectively, represent fieldlike (FL) and dampinglike (DL) torques.

plane, which is consistent with the pattern of other oriented Mn_3Pt.

For comparing the dependence of σ_z-induced atypical torques on current direction, we summarize the torque ratios τ_B/τ_A and τ_C/τ_S for differently oriented Mn_3Pt in Table S2 [21] and display these data in Fig. 6. Panels (a), (b), and (c) correspond to the (100)-, (110)-, and (111)-oriented Mn_3Pt, respectively. Obviously, the atypical σ_z shows strong dependence on the current direction. The τ_z/τ_y ratios for both fieldlike (FL) and dampinglike (DL) torques are larger for current along the [011], [1$\bar{1}$0], and [1$\bar{1}$0] directions (parallel to the magnetic mirror planes), respectively, for (100)-, (110)-, and (111)-oriented Mn_3Pt, indicating robust generation of σ_z only occurs when the current is parallel to the magnetic mirror plane.

The charge to spin conversion efficiency of Mn_3Pt is discussed in the Supplemental Material [21]. It is found that the spin Hall angle (SHA) of Mn_3Pt has strong orientation dependence, wherein (100)-oriented Mn_3Pt has the largest value. This dependence was also observed in Mn_3Ir [8], which is ascribed to the noncollinear magnetic configuration [32,33]. The SHA of (100)-oriented Mn_3Pt is larger than that of Pt, giving rise to lower critical switching current density (Fig. S6 [21]), indicating Mn_3Pt is a promising material in spintronics devices.

IV. CONCLUSION

In conclusion, we deposited three differently oriented Mn_3Pt films with T_2 magnetic configuration and carried out ST FMR measurements for Mn_3Pt/Py bilayers. In this system, we observed robust generation of out of plane spin polarization (σ_z), which shows strong dependence on magnetic mirror symmetry. Current parallel (perpendicular) to the magnetic mirror plane induces strong (weak) generation of σ_z in all three differently oriented Mn_3Pt films. We theoretically analyzed the dependence of magnetic symmetry on the generation of σ_z, which is well consistent with our experimental results. Our results not only provide a better understanding of controllable SOT via magnetic symmetry in noncollinear antiferromagnets, but also pave the way for field-free magnetization switching and next-generation magnetic memories.

ACKNOWLEDGMENTS

This work is supported by the National Natural Science Foundation of China (Grant No. 51871130) and the Natural Science Foundation of Beijing, China (Grant No. JQ20010). C.S. acknowledges the support of Beijing Innovation Center for Future Chip (ICFC), Tsinghua University.

[1] L. Liu, C. F. Pai, Y. Li, H. W. Tseng, D. C. Ralph, and R. A. Buhrman, Spin-torque switching with the giant spin Hall effect of tantalum, Science **336**, 555 (2012).

[2] I. M. Miron, K. Garello, G. Gaudin, P. J. Zermatten, M. V. Costache, S. Auffret, S. Bandiera, B. Rodmacq, A. Schuhl, and P. Gambardella, Perpendicular switching of a single ferromagnetic layer induced by in-plane current injection, Nature (London, U.K.) **476**, 189 (2011).

[3] L. Liu, O. J. Lee, T. J. Gudmundsen, D. C. Ralph, and R. A. Buhrman, Current-Induced Switching of Perpendicularly Magnetized Magnetic Layers Using Spin Torque From the Spin Hall Effect, Phys. Rev. Lett. **109**, 096602 (2012).

[4] A. Manchon, J. Železný, I. M. Miron, T. Jungwirth, J. Sinova, A. Thiaville, K. Garello, and P. Gambardella, Current-induced spin-orbit torques in ferromagnetic and antiferromagnetic systems, Rev. Mod. Phys. **91**, 035004 (2019).

[5] C. Song, R. Q. Zhang, L. Y. Liao, Y. J. Zhou, X. F. Zhou, R. Y. Chen, Y. F. You, X. Z. Chen, and F. Pan, Spin-orbit torques: Materials, mechanisms, performances, and potential applications, Prog. Mater. Sci. **118**, 100761 (2021).

[6] Y. Wang, D. Zhu, Y. Wu, Y. Yang, J. Yu, R. Ramaswamy, R. Mishra, S. Shi, M. Elyasi, K. L. Teo, Y. Wu, and H. Yang, Room temperature magnetization switching in topological insulator-ferromagnet heterostructures by spin-orbit torques, Nat. Commun. **8**, 1364 (2017).

[7] S. Husain, R. Gupta, A. Kumar, P. Kumar, N. Behera, R. Brucas, S. Chaudhary, and P. Svedlindh, Emergence of spin-orbit torques in 2D transition metal dichalcogenides: A status update, Appl. Phys. Rev. **7**, 041312 (2020).

[8] W. Zhang, W. Han, S. H. Yang, Y. Sun, Y. Zhang, B. Yan, and S. S. P. Parkin, Giant facet-dependent spin-orbit torque and spin Hall conductivity in the triangular antiferromagnet $IrMn_3$, Sci. Adv. **2**, e1600759 (2016).

[9] D. MacNeill, G. M. Stiehl, M. H. D. Guimaraes, R. A. Buhrman, J. Park, and D. C. Ralph, Control of spin-orbit torques through crystal symmetry in WTe_2/ferromagnet bilayers, Nat. Phys. **13**, 300 (2017).

[10] D. Macneill, G. M. Stiehl, M. H. D. Guimarães, N. D. Reynolds, R. A. Buhrman, and D. C. Ralph, Thickness dependence of spin-orbit torques generated by WTe_2, Phys. Rev. B **96**, 054450 (2017).

[11] M. H. D. Guimarães, G. M. Stiehl, D. MacNeill, N. D. Reynolds, and D. C. Ralph, Spin-orbit torques in $NbSe_2$/permalloy bilayers, Nano Lett. **18**, 1311 (2018).

[12] G. M. Stiehl, D. MacNeill, N. Sivadas, I. El Baggari, M. H. D. Guimarães, N. D. Reynolds, L. F. Kourkoutis, C. J. Fennie, R. A. Buhrman, and D. C. Ralph, Current-induced torques with Dresselhaus symmetry due to resistance anisotropy in 2D materials, ACS Nano **13**, 2599 (2019).

[13] J. Zhou, X. Y. Shu, Y. H. Liu, X. Wang, W. N. Lin, S. H. Chen, L. Liu, Q. D. Xie, T. Hong, P. Yang, B. H. Yan, X. F. Han, and J. S. Chen, Magnetic asymmetry induced anomalous spin-orbit torque in IrMn, Phys. Rev B **101**, 184403 (2020).

[14] X. Chen, S. Shi, G. Shi, X. Fan, C. Song, X. Zhou, H. Bai, L. Liao, Y. Zhou, H. Zhang, A. Li, Y. Chen, S. Jiang, Z. Zhu, H. Wu, X. Wang, and D. Xue, Observation of the antiferromagnetic spin Hall effect, Nat. Mater. **20**, 800 (2021).

[15] T. Nan, C. X. Quintela, J. Irwin, G. Gurung, D. F. Shao, J. Gibbons, N. Campbell, K. Song, S. Y. Choi, L. Guo, R. D. Johnson, P. Manuel, R. V. Chopdekar, I. Hallsteinsen, T. Tybell, P. J. Ryan, J. W. Kim, Y. Choi, P. G. Radaelli, D. C. Ralph *et al.*, Controlling spin current polarization through non-collinear antiferromagnetism, Nat. Commun. **11**, 4671 (2020).

[16] L. Liu, C. H. Zhou, X. Shu, C. Li, T. Zhao, W. Lin, J. Deng, Q. Xie, S. Chen, J. Zhou, R. Guo, H. Wang, J. Yu, S. Shi, P. Yang, S. Pennycook, A. Manchon, and J. Chen, Symmetry-dependent field-free switching of perpendicular magnetization, Nat. Nanotechnol. **16**, 277 (2021).

[17] S. Nakatsuji, N. Kiyohara, and T. Higo, Large anomalous Hall effect in a non-collinear antiferromagnet at room temperature, Nature (London, UK) **527**, 212 (2015).

[18] M. Ikhlas, T. Tomita, T. Koretsune, M. T. Suzuki, D. Nishio-Hamane, R. Arita, Y. Otani, and S. Nakatsuji, Large Anomalous Nernst effect at room temperature in a chiral antiferromagnet, Nat. Phys. **13**, 1085 (2017).

[19] E. Kren, G. Kadar, L. Pal, J. Solyom, P. Szabo, and T. Tarnoczi, Magnetic structures and exchange interactions in the Mn-Pt System, Phys. Rev. **171**, 574 (1968).

[20] J. Kubler, K. H. Hock, J. Sticht, and A. R. Williams, Density functional theory of non-collinear magnetism, J. Phys. F **18**, 469 (1988).

[21] See Supplemental Material at http://link.aps.org/supplemental/10.1103/PhysRevB.104.104401 for more details regarding the calibration of relative orientation between current and magnetic mirror; symmetric analysis of spin operator matrices; resistivity and magnetization measurements; calculation of SHA, $4\pi M_{\text{eff}}$, α, and strain; and the line-shape separation process.

[22] Z. Q. Liu, H. Chen, J. M. Wang, J. H. Liu, K. Wang, Z. X. Feng, H. Yan, X. R. Wang, C. B. Jiang, J. M. D. Coey, and A. H. Macdonald, Electrical switching of the topological anomalous Hall effect in a non-collinear antiferromagnet above room temperature, Nat. Electron. **1**, 172 (2018).

[23] X. Chen, X. Zhou, R. Cheng, C. Song, J. Zhang, Y. Wu, Y. Ba, H. Li, Y. Sun, Y. You, Y. Zhao, and F. Pan, Electric field control of Néel spin–orbit torque in an antiferromagnet, Nat. Mater. **18**, 931 (2019).

[24] M. T. Suzuki, T. Koretsune, M. Ochi, and R. Arita, Cluster multipole theory for anomalous Hall effect in antiferromagnets, Phys. Rev. B **95**, 094406 (2017).

[25] M. Seeman, D. Ködderitzsch, S. Wimmer, and H. Ebert, Symmetry-imposed shape of linear response tensors, Phys. Rev. B **92**, 155138 (2015).

[26] H. Chen, Q. Niu, and A. H. MacDonald, Anomalous Hall Effect Arising from Noncollinear Antiferromagnetism, Phys. Rev. Lett. **112**, 017205 (2014).

[27] X. D. Zhou, J. P. Hanke, W. X. Feng, F. Li, G. Y. Guo, Y. G. Yao, S. Blüge, and Y. Mokrousov, Spin-order dependent anomalous Hall effect and magneto-optical effect in the noncollinear antiferromagnets Mn_3XN with X = Ga, Zn, Ag, or Ni, Phys. Rev. B **99**, 104428 (2019).

[28] I. Samathrakis, and H. B. Zhang, Tailoring the anomalous Hall effect in the noncollinear antiperovskite Mn_3GaN, Phys. Rev. B **101**, 214423 (2020).

[29] G. Gurung, D. F. Shao, T. R. Paudel, and E. Y. Tsymbal, Anomalous Hall conductivity of noncollinear magnetic antiperovskites, Phys. Rev. Mater. **3**, 044409 (2019).

[30] N. Mecking, Y. S. Gui, and C. M. Hu, Microwave photovoltage and photoresistance effects in ferromagnetic microstrips, Phys. Rev. B **76**, 224430 (2007).

[31] L. Liu, T. Moriyama, D. C. Ralph, and R. A. Buhrman, Spin-Torque Ferromagnetic Resonance Induced by the Spin Hall Effect, Phys. Rev. Lett. **106**, 036601 (2011).

[32] Y. Zhang, Y. Sun, H. Yang, J. Železný, S. P. P. Parkin, C. Felser, and B. Yan, Strong anisotropic anomalous Hall effect and spin Hall effect in the chiral antiferromagnetic compounds Mn_3X (X = Ge, Sn, Ga, Ir, Rh, and Pt), Phys. Rev. B **95**, 075128 (2017).

[33] J. Železný, Y. Zhang, C. Felser, and B. Yan, Spin-Polarized Current in Noncollinear Antiferromagnets, Phys. Rev. Lett. **119**, 187204 (2017).